Title
Use of Fast Ion D-Alpha diagnostics for understanding ICRF effects

Journal
AIP Conference Proceedings, 1187(1)

ISSN
0094-243X

ISBN
978-0-7354-0753-4

Authors
Podestà, M
Heidbrink, WW
Liu, D
et al.

Publication Date
2009-11-26

DOI
10.1063/1.3273840

Use of Fast Ion D-Alpha diagnostics for understanding ICRF effects

M. Podestà*, W. W. Heidbrink*, D. Liu*, Y. Luo*, E. Ruskov*, R .E. Bell†, E. D. Fredrickson†, J. C. Hosea†, S. S. Medley†, K. H. Burrell**, M. Choi**, R. I. Pinsker** and R. W. Harvey‡

*University of California Irvine, Irvine CA - USA
†Princeton Plasma Physics Laboratory, Princeton NJ - USA
**General Atomics, P.O. Box 85608, San Diego CA - USA
‡CompX, Del Mar, CA - USA

Abstract. Combined neutral beam injection and fast wave heating at cyclotron harmonics accelerate deuterium fast ions in the National Spherical Torus Experiment (NSTX) and in the DIII-D tokamak. Acceleration above the injected energy is evident in fast-ion D-alpha (FIDA) and volume-average neutron data. The FIDA diagnostic measures spatial profiles of the accelerated fast ions. In DIII-D, the acceleration is at a 4th or 5th cyclotron harmonic; the maximum enhancement in the high-energy FIDA signal is 8-10 cm beyond the resonance layer. In NSTX, acceleration is observed at five harmonics (7-11) simultaneously; overall, the profile of accelerated fast ions is much broader than in DIII-D. The energy distribution predicted by the CQL3D Fokker-Planck code agrees fairly well with measurements in DIII-D. However, the predicted profiles differ from experiment, presumably because the current version of CQL3D uses a zero-banana-width model.

Keywords: Tokamak, ICRF, High harmonic fast wave, heating, current drive, fast ion D-alpha
PACS: 52.25.Xz, 52.50.Qt, 52.70.Kz

INTRODUCTION

Injection of radio-frequency (rf) waves is one of the methods envisaged to heat a magnetically confined fusion plasma and sustain a non-inductive plasma current. In particular, waves with frequency corresponding to harmonics of the ion cyclotron resonant frequency (ICRF) have been proven as an attractive mean to heat the electron population, drive a non-inductive current via directed injection and modify the safety factor profile [1]. Such schemes are commonly known as *high-harmonic fast wave* (HHFW) heating and current-drive, as the *fast* branch of the rf wave [2] is coupled to the plasma by means of an antenna located at the plasma edge. Although the primary damping of HHFW occurs on thermal electrons [3], parasitic absorption can take place through cyclotron resonance on a pre-existing suprathermal (or *fast*) ion population, such as that generated by neutral beam (NB) injection. From the point of view of heating and current drive, this represents a loss of efficiency, as part of the available power is dispersed into spurious channels. On the other hand, fast ions can have stabilizing or destabilizing effect on different classes of instabilities [4][5]. Understanding how HHFW power is transfered to fast ions, and the properties of the resulting fast ion distribution, might thus be relevant for instability control purposes.
The details of the fast ion profile and velocity distribution after acceleration by HHFW

CP1187, *Radio Frequency Power in Plasmas*
edited by V. Bobkov and J.-M. Noterdaeme

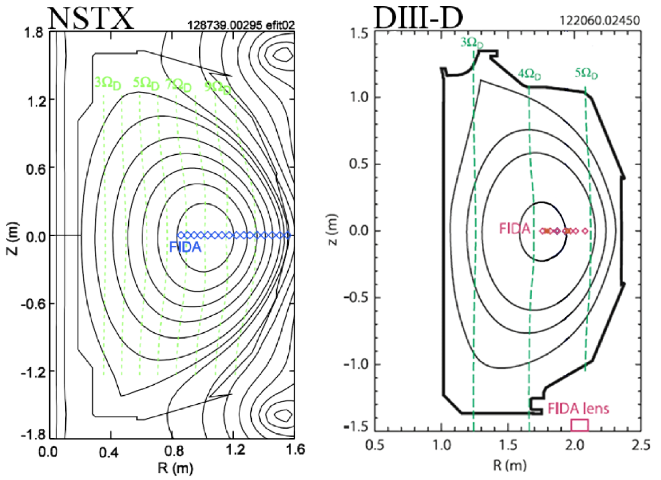

FIGURE 1. Poloidal cross-section of NSTX (left) and DIII-D (right). The green dashed lines indicate the HHFW resonant layers at the different harmonics. Symbols refer to the interceptions of the FIDA views at the midplane.

are expected to depend on both the number of resonances involved in the absorption process, and on the initial fast ion distribution parameters such as energy and Larmor radius, ρ_f. A better understanding of ICRF waves propagation and absorption mechanisms may greatly benefit from experiments performed under very different conditions. In this paper, we focus on the characterization of fast ion acceleration by ICRF waves on a conventional aspect ratio tokamak, DIII-D [6], and on a small aspect ratio device, NSTX [7]. The two machines differ considerably in the number of resonances that are simultaneously accessible, mainly because of the different magnetic field configuration. More specifically, the low aspect ratio of NSTX allows the presence of multiple, closely spaced resonances spanning the entire poloidal cross section, whereas a maximum of three resonances, much more widely spaced in major radius, are typically present in DIII-D plasmas, as shown in Fig. 1. Another major difference is the magnitude of the magnetic field, which makes the term $k_\perp \rho_f$ much larger on NSTX than on DIII-D ($k_\perp$ is the perpendicular wavenumber of the propagating waves). As a reference, $\rho_f \leq 3$ cm in DIII-D and $\rho_f \leq 20$ cm on NSTX. Fast ion acceleration by ICRF waves has been already observed on both machine in past years [8][9]. Since then, a set of Fast-Ion D-Alpha (FIDA) spectroscopic diagnostics has become routinely available on both devices, allowing more detailed studies of the response of fast ions to HHFW injection.

The paper is organized as follows. First, the principles of FIDA spectroscopy are discussed. The experimental setup and the FIDA systems installed on NSTX and DIII-D are described. Then, the experimental observations on HHFW absorption by fast ions on the two devices are presented, including a comparison with the predictions of the bounce-averaged Fokker-Planck code CQL3D [10] for the DIII-D data. Finally, the results are summarized and discussed.

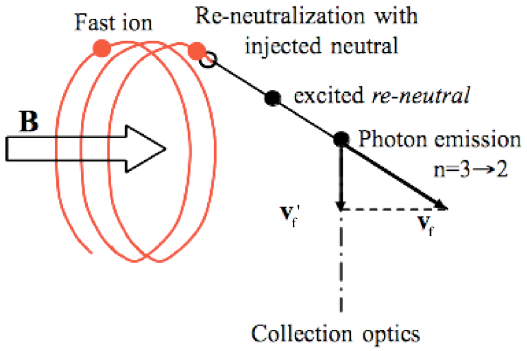

FIGURE 2. Principles of FIDA spectroscopy. A fast ion recombines with an injected neutral, then emits a photon. For a $3 \rightarrow 2$ transition, the observed wavelength is Doppler-shifted with respect to the cold D_α by virtue of its high velocity compared to the thermal ions. The Doppler shift is determined by the *projection* of the velocity along the line of sight.

EXPERIMENTAL SETUP AND DIAGNOSTICS

Principles of Fast-Ion D-Alpha (FIDA) spectroscopy

Fast ions that travel in a region illuminated by a neutral beam can undergo charge-exchange reactions with the injected neutrals (Fig. 2). The recombining fast ions undergoing a $3 \rightarrow 2$ transition emit photons with wavelength in the D_α (or Balmer-alpha) range. Due to their higher energy compared to the thermal ions, light from recombining fast ions appears in the blue- and red-shifted tails of the D_α spectrum [11]. Fast Ion D-Alpha (FIDA) diagnostics are aimed at measuring these tails of the D_α spectrum. The resulting signal is given by

$$s = s_f + B, \quad s_f(\lambda) \equiv \int\int W F_f \, dE \, dp \tag{1}$$

where $B > s_f$ is the background light not associated with fast ions, e.g. from cold D_α, bremsstrahlung and impurities, and s_f is the fast ion signal [9]. $F_f(E,p)$ is the local fast ion distribution function. E and $p = v_{f,\parallel}/v_f$ are the energy and pitch parameter (v_f is the fast ion velocity and $v_{f,\parallel}$ its component along the magnetic field). The *response function*, $W(E,p)$, accounts for an effective averaging over the phase-space [9], for the specific viewing and beam geometry, and for the recombination rate of fast ions. Therefore, $W \propto F_b < \sigma_{cx}|\mathbf{v}| >$, where F_b is the local distribution of injected neutrals, $\mathbf{v}$ the relative (impact) velocity and σ_{cx} the charge-exchange cross section. The wavelength λ is related to the energy of the measured photons, E_λ, via the Doppler-shift formula $\lambda = \lambda_0 \left(1 \pm v'_f/c\right)$. Here λ_0 is the wavelength of the cold D_α line, c is the speed of light and v'_f is the projection of the recombined fast ion velocity along the line-of-sight (Fig. 2). Equation 1 implies that the measured spectrum is a one-dimensional sampling

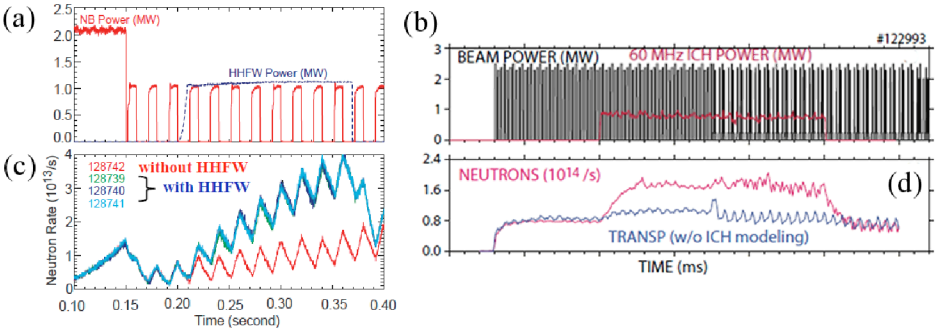

FIGURE 3. Waveform of injected NB and rf power in NSTX (a) and DIII-D (b). The measured volume-integrated neutron rate is shown in (c-d).

of $F_f(E,p)$, convolved with the response function, W. The complete expression of W can be determined numerically through a simulation code (cf. the Appendixes in Refs. [9] and [12]). For practical purposes, the integrated fast-ion signal is instead approximated as $\int_{\Delta\lambda} s_f d\lambda \propto n_f n_b < \sigma_{cx} \overline{v} >$, from which the density n_f is calculated from the experimental data. The integral is performed over the wavelength range, $\Delta\lambda$, corresponding to the expected fast-ion energy range. $\overline{v}$ is an average impact velocity, with σ_{cx} a smooth function of $\overline{v}$. The local beam neutral density, n_b, is calculated through a beam-attenuation code. We refer to n_f as the *FIDA density*, to highlight that (i) it represents a sampling of the fast ion density through the response function, W, and (ii) it is only an approximate representation of the actual fast ion density. Since the FIDA lines of sight on both NSTX and DIII-D are almost perpendicular to the total magnetic field, the resulting signal is weighted toward the perpendicular fast ion velocities.

Experimental setup

The NSTX plasmas investigated here have peak electron density $n_e \approx 3 \times 10^{19}$ m^{-3}, and ion and electron temperature $T_i \approx T_e \leq 1$ keV. The magnetic field and plasma current are 0.55 T and 800 kA, respectively. From 150 ms to 400 ms the NB injected power is 1 MW, with 50% duty-cycle modulation of the source (period 20 ms), see Fig. 3-a. The injection energy is 65 keV. In addition, ≈ 1.1 MW of rf power at f=30 MHz is injected from 210 ms to 370 ms via a twelve-strap antenna located close to the plasma edge. The straps are fed by six transmitters, which are phase-controlled through a feedback loop. The parallel (to the magnetic field) wavenumber spectrum coupled to the plasma edge is $k_{\|} = 7$ m^{-1}, that corresponds to waves propagating mostly in the co-current direction [1]. The FIDA system measures spectra in the D_α range with 5 cm spatial resolution, ≈ 10 keV spectral resolution, and 10 ms temporal resolution. It covers the range 85 $\rightarrow$ 155 cm along the major radius (Fig. 1). NB modulation is used to calculate the background [12]. More details on the NSTX FIDA systems are found in Ref. [13].
DIII-D plasmas used in this study have electron density $n_e \leq 2 \times 10^{19}$ m^{-3}. The tempera-

ture is $T_i \leq T_e \leq 3$ keV. The value of the toroidal magnetic field is 1.9 T. The average NB power is 1.2 MW from sources with tangency radii of 0.76 m and 1.15 m and maximum acceleration voltage of 84 kV. The NB power is modulated with 50% duty cycle (Fig. 3-b). Fast waves are injected through a four-element antenna. Up to 1 MW of total power is delivered by the transmitter, operating at 60 MHz. The parallel wavenumber spectrum is peaked at $k_{\|} \approx 5$ m^{-1}. A dedicated FIDA system, measuring the entire D_α spectrum, is installed [11]. It is capable of measuring two channels in a single shot, with the possibility of switching fibers from shot to shot to cover an extended radial range (Fig. 1). As for the NSTX systems, the lines of sight are looking vertically through the plasma. Additional measurements are obtained from the system commonly used on DIII-D for charge-exchange recombination spectroscopy, for a total of nine channels available in the same shot. In this case, measurements are typically limited to the blue-shifted portion of the D_α spectrum, which is less contaminated by impurity lines. The background is calculated from the off phases of NB modulation. As a reference in the experiment-modeling comparison, the plasma profiles and neutron rate are obtained from the plasma equilibrium code TRANSP code [14], not including fast ion acceleration by ICRF. The fast ion distribution during HHFW injection is modeled by means of the CQL3D code. It is then used as input in a forward-modeling FIDA simulation code [9][12], which reconstructs the "measured" FIDA signal. The latter is finally compared with the experimental data to verify the consistency of the models' assumptions.

EXPERIMENTAL RESULTS

The main results obtained on NSTX are summarized in Figs. 3 and 4 [15]. For comparison, data from a reference discharge with the same NB timing and power but without HHFW injection is shown. Typically, the no-rf case is characterized by slightly lower density and electron temperature. A time window from 290 ms to 360 ms is selected to average the measured fast ion profiles and spectra. A first indication of the enhancement in the higher energy fast ion population is provided by neutron rate measurements, which show an increase by a factor three as the rf is turned on compared to the no-rf case (Fig.3-c). A confirmation is provided by FIDA spectra, showing higher count rates for energies > 20 keV. In particular, an enhancement above the NB injection energy is observed (Fig.4-a). Compared to the no-rf case, the radial profile of fast ions is also enhanced over a broad spatial region (Fig.4-b). The relative increase in the profile is quantified in Fig.4-c. The FIDA spectra are integrated over the range $E_\lambda \in [30,65]$ keV. An increase by at least a factor 2 is observed on almost all the channels. For the central channels, corresponding to measurements at $R = 85 \rightarrow 105$ cm along the major radius, the enhancement is as high as a factor 3.5. In the same figure, the positions of the HHFW resonances lying inside the plasma volume are shown. Moving outward from the center, they correspond to the $7 \rightarrow 11$ harmonics of the fundamental ion cyclotron frequency. Preliminary results from simulations based on the CQL3D indicate that the agreement with the experiments is poor for both the spectral features and the spatial profiles of accelerated fast ions [15]. The most likely reason for this discrepancy is the zero-banana width assumed by CQL3D, which is a poor approximation for the low-aspect-ratio, large-ρ_f regime in which NSTX operates.

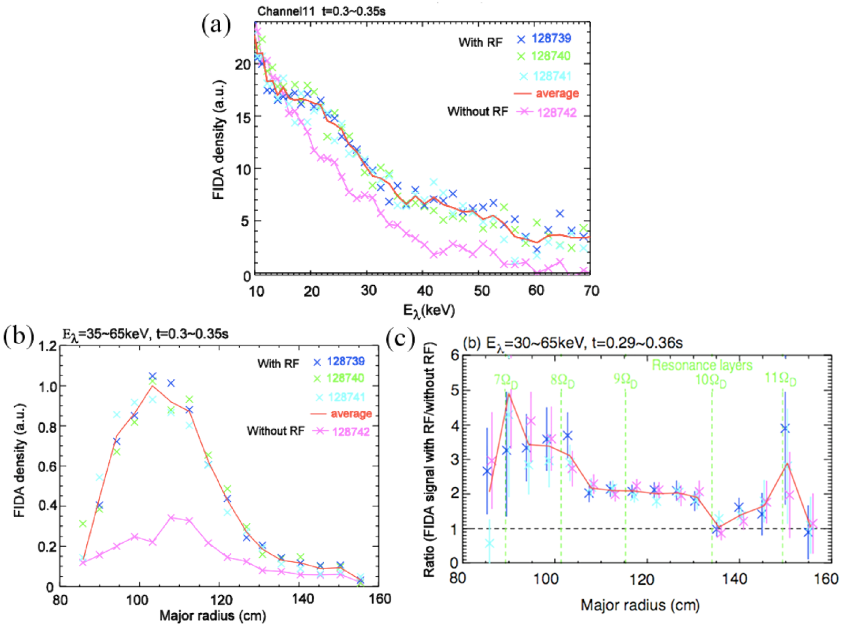

FIGURE 4. FIDA measurements of fast ion profiles on NSTX for the cases with and without rf injection [adapted from ref. [15]]. Three nominally identical shots are shown for the rf case. (a) Spectra measured at $R \approx 1$ m, close to the magnetic axis. (b) Spatial fast ion density profiles, showing a large increase during rf injection over virtually all the radial positions. (c) Relative increase in the spatial profile with respect to the no-rf case. The vertical dashed lines indicate the position of the IC resonances.

Qualitatively similar results are obtained on DIII-D, as summarized in Figs. 3 and 5 [9]. After the rf is turned on, the neutron rate increases by a factor 2 (Fig. 3-d), which is not reproduced by TRANSP without including ICRF acceleration of fast ions. This excludes that the increase is due to modifications of the plasma profiles. The enhancement in the neutron rate is about 50% less than on NSTX. The FIDA spectra exhibit enhanced tails during the rf phase (Fig. 5-a). For 5th harmonic acceleration, the relative increase with respect to the no-rf case is in good agreement with simulations based on the fast ion distribution calculated by CQL3D. (No simulations have been performed for the 4th harmonic case). For 4th and 5th harmonic heating, the fast ion pressure profile from CQL3D agrees with the measured one for regions far from the resonance (Fig. 5-b), but the agreement becomes marginal as the resonant layer is approached, i.e. close to the plasma center. The main difference between the two devices is found in the spatial profile of accelerated fast ions (Fig. 5-c). For both 4th and 5th harmonic resonances, the broadening is much narrower on DIII-D than in NSTX, where multiple resonances participate in the wave absorption process. The single active resonance in DIII-D allows one to observe a systematic outward shift by $8-10$ cm of the peak in the enhancement with respect to the nominal resonance position. For the 5th harmonic resonance, CQL3D modeling accounts only in part for this shift.

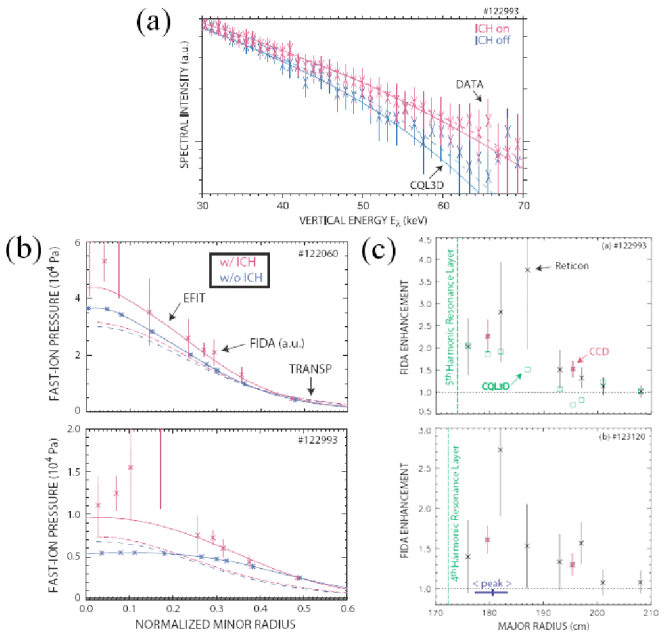

FIGURE 5. FIDA measurements of fast ion profiles on DIII-D, with and without rf injection [adapted from Ref. [9]]. (a) Spectra measured at $R \approx 1.8$ m during 5th harmonic heating, and comparison with CQL3D predictions. (b) Spatial fast ion pressure profiles and comparison with TRANSP modeling. (c) Relative increase in the spatial profile with respect to the no-rf case for 4th and 5th harmonic heating.

SUMMARY AND DISCUSSION

In summary, fast ion acceleration by HHFW during NB injection has been documented on a conventional and a low aspect-ratio device. As predicted by theory, and reported from previous experiments, a fast ion tail extending above the NB injection energy forms. FIDA spectroscopic diagnostics have proven to be a powerful tool to characterize the resulting fast ion distribution in energy, time and space. As expected from theory [3] and verified experimentally [9], HHFW absorption by fast ions increases with $k_\perp \rho_f$. This explains the strong absorption on NSTX, where ρ_f can be as large as 20 cm, compared to ~ 2 cm on DIII-D. From the point of view of heating and current drive, fast ion absorption may represent a loss channel that competes efficiently with absorption on the bulk electrons, and so must be accounted for in simulations.

The measured spatial profile of accelerated fast ions differs considerably for the two cases. A broad profile is measured on NSTX, where multiple resonances are simultaneously accessible to the rf waves. In DIII-D, where a single ICRF harmonic resonance is usually active, the profiles appear narrower. The comparison between experimental and simulated profiles using CQL3D show qualitative and quantitative discrepancies. On DIII-D, FIDA spectra are in fair agreement with the simulations, but the model can not reproduce the observed position of the peak in the spatial profiles of accelerated fast

ions. The reason is likely due to finite Larmor radius and banana-width effects, which are not included the code. Recent simulations based on the drift-orbit code ORBIT-RF [16], capable of treating finite-banana width correctly, seem to confirm this interpretation. A similar modeling work is ongoing for the NSTX case; the results will be reported in a future publication [15]. Future experiments on NSTX and DIII-D will further benefit from upgraded FIDA diagnostics to improve the understanding of rf interaction with fast ions. At the same time, improvements to the existing codes are planned to include important physics such as the finite-banana width effects.

ACKNOWLEDGMENTS

The assistence of the NSTX and DIII-D teams is gratefully acknowledged. Work supported by the US DOE under SC-G903402, DE-FC02-04ER54698, DE-AC02-76CH03073, and DE-FG03-99ER54541.

REFERENCES

1. C. K. Phillips, R. E. Bell, L. A. Berry, P. T. Bonoli, R. W. Harvey, J. C. Hosea, E. F. Jaeger, B. P. LeBlanc, P. M. Ryan, G. Taylor, E. J. V. J. B. Wilgen, J. R. Wilson, J. C. Wright, H. Yuh, and NSTX Team, *Nucl. Fusion*, **49**, 075015 (2009).
2. T. Stix, *The theory of plasma waves*, McGraw-Hill, 1962.
3. M. Ono, *Phys. Plasmas*, **2**, 4075 (1995).
4. W. W. Heidbrink, E. D. Fredrickson, T. K. Mau, C. C. Petty, R. I. Pinsker, M. Porkolab, and B. W. Rice, *Nucl. Fusion*, **39**, 1369 (1999).
5. W. W. Heidbrink, E. Ruskov, E. D. Fredrickson, N. Gorelenkov, S. S. Medley, H. L. Berk, and R. W. Harvey, *Plasma Phys. Control. Fusion*, **48**, 1347 (2006).
6. J. L. Luxon, *Nucl. Fusion.*, **42**, 614 (2002).
7. M. Ono, S. M. Kaye, Y.-K. M. Peng, G. Barnes, W. Blanchard, M. D. Carter, J. Chrzanowski, L. Dudek, R. Ewig, D. Gates, R. E. Hatcher, T. Jarboe, S. C. Jardin, D. Johnson, R. Kaita, M. Kalish, C. E. Kessel, H. W. Kugel, R. Maingi, R. Majeski, J. Manickam, B. McCormack, J. E. Menard, D. Mueller, B. A. Nelson, B. E. Nelson, C. Neumeyer, G. Oliaro, F. Paoletti, R. Parsells, E. Perry, N. Pomphrey, S. Ramakrishnan, R. Raman, G. Rewoldt, J. Robinson, A. L. Roquemore, P. Ryan, S. Sabbagh, D. Swain, E. J. Synakowski, M. Viola, M. Williams, J. R. Wilson, and NSTX Team, *Nucl. Fusion*, **40**, 557 (2000).
8. A. L. Rosenberg, J. E. Menard, J. R. Wilson, S. S. Medley, R. Andre, C. K. Phillips, D. S. Darrow, B. P. LeBlanc, M. H. Redi, N. J. Fish, and NSTX Team, *Phys. Plasmas*, **11**, 2441 (2004).
9. W. W. Heidbrink, Y. Luo, K. H. Burrell, R. W. Harvey, R. I. Pinsker, and E. Ruskov, *Plasma Phys. Control. Fusion*, **49**, 1457 (2007).
10. R. W. Harvey, and M. G. McCoy, *Proceedings of the IAEA Technical Committee Meeting on Advanced Simulation and Modeling of Thermonuclear Plasmas (Montreal, 1992)*, Vienna, IAEA, 1992.
11. Y. Luo, W. W. Heidbrink, K. H. Burrell, D. H. Kaplan, and P. Gohil, *Rev. Sci. Instr.*, **78**, 033505 (2007).
12. W. W. Heidbrink, K. H. Burrell, Y. Luo, N. A. Pablant, and E. Ruskov, *Plasma Phys. Control. Fusion*, **46**, 1855 (2004).
13. M. Podestà, W. W. Heidbrink, R. E. Bell, and R. Feder, *Rev. Sci. Instr.*, **78**, 10E521 (2008).
14. R. V. Budny, *Nucl. Fusion*, **34**, 1247 (1994).
15. D. Liu, W. W. Heidbrink, M. Podestà, R. E. Bell, E. D. Fredrickson, S. S. Medley, R. W. Harvey, J. Hosea, and E. Ruskov, *Plasma Phys. Control. Fusion (submitted)* (2009).
16. M. Choi, V. S. Chan, L. A. Berry, E. F. Jaeger, D. Green, P. Bonoli, J. Wright, and RF SciDAC Team, *Phys. Plasmas*, **16**, 052513 (2009).